Accepted Manuscript

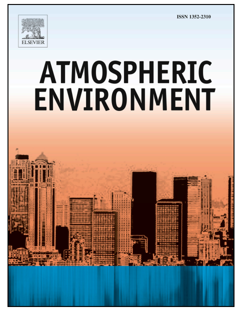

Assimilating aircraft-based measurements to improve Forecast Accuracy of Volcanic Ash Transport

G. Fu, H.X. Lin, A.W. Heemink, A.J. Segers, S. Lu, T. Palsson

PII: S1352-2310(15)30132-1

DOI: 10.1016/j.atmosenv.2015.05.061

Reference: AEA 13868

To appear in: *Atmospheric Environment*

Received Date: 22 December 2014

Revised Date: 26 May 2015

Accepted Date: 27 May 2015

Please cite this article as: Fu, G., Lin, H.X., Heemink, A.W., Segers, A.J., Lu, S., Palsson, T., Assimilating aircraft-based measurements to improve Forecast Accuracy of Volcanic Ash Transport, *Atmospheric Environment* (2015), doi: 10.1016/j.atmosenv.2015.05.061.

Assimilating aircraft-based measurements to improve Forecast Accuracy of Volcanic Ash Transport

G. Fu[a,*], H.X. Lin[a], A.W. Heemink[a], A.J. Segers[b], S.Lu[a], T. Palsson[c]

[a] *Dept. of Applied Mathematics, Delft University of technology, Mekelweg 4, 2628 CD Delft, The Netherlands*
[b] *TNO, Dept. of Climate, Air and Sustainability, P.O. Box 80015, 3508 TA Utrecht, the Netherlands*
[c] *School of Science and Engineering, Reykjavik University, 101 Reykjavik, Iceland*

Abstract

The 2010 Eyjafjallajökull volcano eruption had serious consequences to civil aviation. This has initiated a lot of research on volcanic ash transport forecast in recent years. For forecasting the volcanic ash transport after eruption onset, a volcanic ash transport and diffusion model (VATDM) needs to be run with Eruption Source Parameters (ESP) such as plume height and mass eruption rate as input, and with data assimilation techniques to continuously improve the initial conditions of the forecast. Reliable and accurate ash measurements are crucial for providing a successful ash clouds advice. In this paper, simulated aircraft-based measurements, as one type of volcanic ash measurements, will be assimilated into a transport model to identify the potential benefit of this kind of observations in an assimilation system. The results show assimilating aircraft-based measurements can significantly improve the state of ash clouds, and further providing an improved forecast

*Corresponding author. Tel.: +31(0)687241152; Fax: +31 15 278 7295.
Email address: G.Fu@tudelft.nl (G. Fu)

as aviation advice. We also show that for advice of aeroplane flying level, aircraft-based measurements should be preferably taken from this level to obtain the best performance on it. Furthermore it is shown that in order to make an acceptable advice for aviation decision makers, accurate knowledge about uncertainties of ESPs and measurements is of great importance.

Keywords: volcanic ash forecast, aircraft-based measurements, data assimilation, uncertainties

1. Introduction

The volcanic activity of Eyjafjallajökull in Iceland in 2010 (Figure 1) has revealed that air traffic is highly vulnerable to volcanic eruptions. Aerosols and ash from eruptions not only reduce visibility for visual navigation, but microscopic glass-rich debris accumulates and melts in the heat of aircraft turbine engines, which eventually leads to engine failure. Most of the volcanic ash from the Eyjafjallajökull eruption on April 14, 2010 and the following days was carried by prevailing winds in South-East direction, provoking a dramatic collapse of European air traffic during several days. Preliminary estimates of the direct and indirect costs that can be attributed to disruption of air travel in Europe as a consequence of this volcanic eruption are in the range of several billion Euros.

As a result of the serious consequences on civil aviation, more than 50 volcanologists, meteorologists, atmospheric dispersion modellers, and space and ground-based monitoring specialists from 12 different countries (including representatives from 6 Volcanic Ash Advisory Centers and related institutions) gathered at the Weather Meteorology Organization (WMO) head-

Figure 1: Eyjafjallajökull volcano eruption plume.

quarters in Geneva, addressing some important research priorities related to Volcanic Ash Transport Forecast problems (Bonadonna et al., 2012). One of the priorities they have identified is to use data assimilation, which refers to the (quasi-) continuous use of observational data to create initial conditions for sequences of model runs. In each assimilation step, a forecast from the previous model run is used as a first guess which is then modified to be in (better) agreement with the observations (Zehner, 2010).

For the purpose of using a data assimilation system to improve the initial conditions of the the ash load, the volcanic ash measurements must be available near-real-time. Flemming and Inness (2013) assimilated for example satellite retrievals in a four-dimensional variation (4D-var) approach. Besides satellite observations of volcanic ashes, many other different scientific measurement campaigns were performed in order to get information about the ash plume, such as using lidars, ceilometers, balloon sondes etc. Among these, also aircraft-based measurements were obtained close to the eruption plume, which are probably the most direct observations possible. In this study, the potential benefit of these kind of observations in an assimilation system is studied. The experiments consist of so-called twin-experiments, where observations are simulated from model simulations and fed into an assimilation system using the same model. In this setup it is a first step towards assimilation of real observations, to obtain a first idea on how to use this kind of observations and what their impact is in an assimilation system.

These aircraft-based data has some advantages compared with satellite data: (1) The aircraft measurement is frequently obtained from the optical particle counters which are equipped on the aircraft, thus the particle concentration observation is real-time and directly detected and it has a higher accuracy. With an error estimate of about 10 percent, which can be achieved by well calibrated instruments (Weber et al., 2012), the accuracy of these observations is high compared to for example satellite data, for which errors 50-60 percent are reported (Zehner, 2010). (2) The aircraft measurement is in-situ which is suitable to be compared directly to a 3-dimensional model state, whereas some other measurements such as satellite data and LIDAR data observe optical properties being accumulated into a single value per vertical column which cannot be compared directly to a 3D model state. (3) An aircraft can decide the route in the sky to follow the ash cloud to always get an appropriate ash concentration. And it can also decide to fly at different altitudes, e.g., if we mainly care about the intercontinental commercial aircraft safety, we can choose to fly at 9 km with a suitable research aircraft (which is commonly the lowest height level for intercontinental commercial planes) to perform measurements. Note that most national and maybe some continental passenger flights are below 9 km altitude, while intercontinental flights are at 9 km and higher altitude.

Currently aircraft-based measurements are only used for validation purpose of volcanic ash clouds (Weber et al., 2012), not yet involved in data assimilation systems. This paper will study the use of aircraft-based measurements in data assimilation with an Ensemble Kalman filter (EnKF) algorithm. This study aims at (1) investigating the performance of aircraft-based measurements in data assimilation systems; (2) study the impact of measurements from different flight altitudes on forecasts at aviation level; (3) discuss the influence of uncertainties in the ESPs and measurements.

This paper is organized as follows. Section 2 gives a brief introduction of volcanic eruption models and introduces the LOTOS-EUROS model used in this study. The validation of LOTOS-EUROS as a VATDM is specified in Section 3. Section 4 gives an introduction of the aircraft-based measurements used in our assimilation experiments. Sequential data assimilation methodology including the stochastic environment and the ensemble-based filter algorithm is presented in Section 5. Section 6 contains the assimilation results and the discussion on the results. Finally, the last section summarizes the concluding remarks of our research.

2. Volcanic eruption models and the LOTOS-EUROS model as VATDM

Numerous volcanic ash transport and dispersion models are available worldwide, and in recent efforts a comparison report among these existing models has been compiled (Bonadonna et al., 2012, 2014). These models are usually off-line coupled to a meteorological model, which require that numerical weather prediction data should be generated first such that the VATD model could use these data. For the transport either Lagrangian or Eulerian approach are used. Some models run quickly such as PUFF (Searcy et al., 1998) can run within minutes and others require many hours to run, such as ATHAM (Oberhuber et al., 1998) requires several days. Several VATD models are used in operational settings, like NAME (Jones et al., 2007) and HYSPLIT (Draxler and Hess, 1998) and therefore are designed to produce volcanic ash simulations quickly for the corresponding volcanic ash advisory center. Inter-comparisons between volcanic ash transport and dispersion models, volcanic ash real-time advisories as well as to the satellite observations have been reported by multiple authors, such as (Witham et al., 2007) and (Webley et al., 2009b).

In our study, the LOTOS-EUROS model is used (Schaap et al., 2008) with model version 1.10. This model is an operational air-quality model, used for daily air quality forecasts over Europe (Curier et al., 2012), focussing on ozone, nitrogen oxides, and particular matter. In addition, it could be configured to simulate transport of tracers in other regions of the world. The model uses the off-line approach and is driven by meteorological data produced by European Centre for Medium-Range Weather Forecasts (ECMWF). The model is used in a tracer mode to produce volcanic ash simulations in a timely and useful manner for forecasting.

To describe a volcanic eruption in LOTOS-EUROS model, Eruption Source Parameters (ESP) such as Plume Height (PH), Mass Eruption Rate (MER), Particle Size Distribution (PSD) and Vertical Mass Distribution (VMD) are needed. In (Mastin et al., 2009) ESPs for different volcanoes are provided as a look up table. LOTOS-EUROS through the add-on initial plume module uses the ESP type data as volcanic emission information for the model forecasting. The LOTOS-EUROS model with volcanic ash configuration has been used to simulate the April 2010 period of activity from Eyjafjallajökull.

The input parameter PH in LOTOS-EUROS is referred from hourly based Icelandic Meteorological Office (IMO) plume height detection (see Figure 2) and usually the uncertainty of PH is taken as 20 % (Bonadonna and Costa, 2013).

For VMD, large explosive volcanic plumes have a typical 'umbrella' shaped vertical distribution (Sparks et al., 1997) and as such this 'umbrella' shaped VMD is adapted into LOTOS-EUROS in this paper, see Figure 3.

The PSD in LOTOS-EUROS is defined in the ESP type S2 as defined by Mastin et al. (2009), in which the mass fraction of erupted debris finer than 63 μm is 0.4. For the S2 type eruption, Durant and Rose (2009) provides the base for the PSD from their analysis of the 1992 Crater Peak, Mount Spurr event. Hence, Table 1 provides the ash distribution based on their analysis and is used by LOTOS-EUROS for its 6 volcanic ash bins.

Another input parameter MER is very hard to measure for an explosive onsetting volcano. Usually it is calculated from plume height. Mastin et al. (2009) did some studies on the parameter relationship and concluded that an empirical relationship between plume height $H(km)$ and eruption rate is

$$H = 2.00V^{0.241}, \tag{1}$$

in which the MER is converted to volumetric flow rate $V(m^3/s)$. For the S2 type eruption, the relationship between volumetric flow rate and MER (kg/s) is (Mastin et al., 2009):

$$\frac{V}{MER} = \frac{1.5e^3}{4.0e^6}. \tag{2}$$

Through PH, Eq. (1) and Eq. (2), MER can be approximately calculated, see Table 2 where PH is specified as that used by Webley et al. (2012) for the WRF-Chem model. Mastin et al. (2009) estimated the uncertainty of MER through this calculation is about 50%.

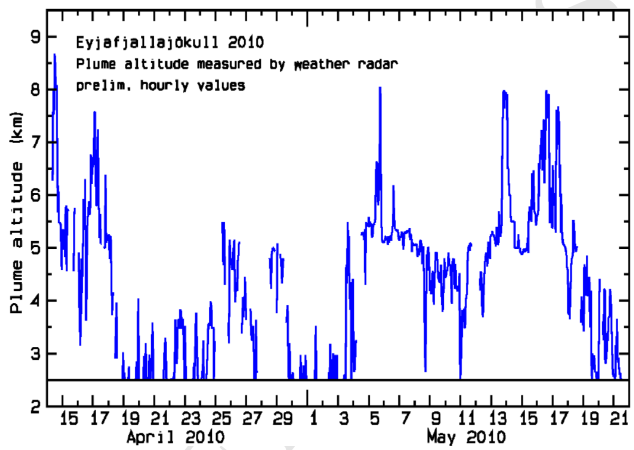

Figure 2: Icelandic Meteorological Office [IMO] plume height detection from April to May, 2010. Courtesy from IMO on-line database.

For the study of Eyjafjallajökull events the model is configured on a domain from 45° to 70° North and 30° West to 15° East covering Iceland and North Europe (Figure 4). The grid resolution is 0.5° longitude × 0.25° latitude, approximately 25 × 25 km. In the vertical the model version used has 12 vertical layers. On top of a surface layer of 25 m, three dynamic layers are present, where the lowest dynamic layer represents the variable mixing layer with the height obtained from the meteorological input, and the upper two dynamic layers are reservoir layers with equal thickness; the top of the

Table 1: Volcanic Ash Particle Size Distribution and ash bins property for LOTOS-EUROS model simulation.

Bins	Particle Diameter	Percent of Mass	Average Particle Size (μm)
vash_1	250 to 2000 μm	29	1125.00
vash_2	63 to 250 μm	31	156.50
vash_3	30 to 63 μm	12	46.50
vash_4	10 to 30 μm	18	20.00
vash_5	2.5 to 10 μm	8	6.25
vash_6	0.0 to 2.5 μm	2	1.25

Table 2: Plume height and Eruption rate in LOTOS-EUROS Model Simulation for April 14-18, 2010. Courtesy from (Webley et al., 2012).

Start Time – End Time	Height ASL (km)	Eruption Rate (kg/s)
4/14 09:00 – 4/14 19:00	9	5.71E+05
4/14 19:00 – 4/15 04:00	5.5	3.87E+04
4/15 04:00 – 4/16 19:00	6	6.44E+04
4/16 19:00 – 4/18 00:00	8.25	3.65E+05

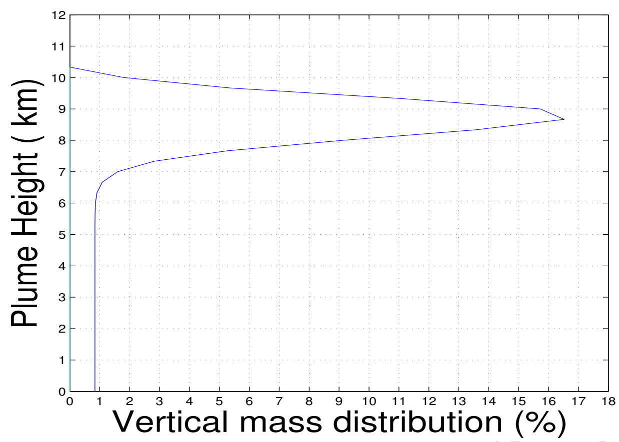

Figure 3: The 'umbrella' vertical mass distribution (VMD) of ash cloud in LOTOS-EUROS. Shown in this case is the vertical profile of an eruption with 10 km plume height.

dynamic layers is set to 3.5 km. The remaining 6 layers have fixed altitudes with equal thickness of 1 km, which set the top to 11.5 km in total.

The volcanic ash concentration is described by 6 aerosol tracers as mentioned above. The physical processes that are relevant for volcanic ash are similar as those that apply for mineral dust, e.g., advective transport and diffusion, deposition, coagulation, sedimentation, and resuspension (Langmann, 2013). Where the transport is determined by the wind fields that could be regarded as rather well known, the other processes deposition and sedimentation processes are rather uncertain. The parameterizations for the later processes involve assumptions on the particle shape for example, which is difficult to summarize in a few numbers. These processes act on the distribution of the total ash mass over the modes (particle sizes) and the total mass load; one could therefore state that almost everything in the description of an ash cloud is uncertain, except for its shape and position. The processes included in this study are transport, sedimentation, and wet- and dry-deposition, where the relevant properties such as average particle size (Table 1) are implemented following Zhang (2001). Processes that are missing yet are for example coagulation, evaporation, and resuspension, which might be considered in future when appropriate observations are available to constrain them, for example sedimentation amounts.

3. Validation for Eyjafjallajökull volcanic ash simulation

Based on the input parameters settings described above, validation with the LOTOS-EUROS model has been made. For the validation experiment, the time period of April 14-18, 2010 is chosen. Figure 4 shows examples of ash plumes simulated by LOTOS-EUROS as well as two other models at two time snapshot 00:00 (UTC) April 15 and 00:00 (UTC) on April 17, 2010. The WRF-Chem results are taken from (Webley et al., 2012) where the WRF-Chem model has been validated as a proper VATDM. For both LOTOS-EUROS and WRF-Chem the figures represent ash mass loadings at selected time, thus the total mass measures over all aerosol modes per area. Figure 4(e) and Figure 4(f) show simulations provided by the Volcanic Ash Advisory Center (VAAC) based on the NAME model. VAAC are set up by the International Civil Aviation Organization (ICAO), to provide information to the aviation community through timely volcanic ash advisories (VAA). For the NAME model the figures show ash cloud locations at specific altitude bounds and ash cloud boundaries in the figures are corresponding to 200 μg m^{-3} which is a very low value by today's standard for aircraft operations (Zehner, 2010). Comparison of NAME model to LOTOS-EUROS and WRF-Chem is made by comparing superposition of ash cloud locations over all the altitude bounds to the boundaries of ash mass loadings.

Table 3: Comparison of Total Mass in KT (10^6 kg) between the LOTOS-EUROS model and the WRF-Chem model simulation of eruption of Eyjafjallajökull volcano in 2010.

Time	LOTOS-EUROS	WRF-Chem
00:00 (UTC) 15 April	11315.45	10648.4
00:00 (UTC) 17 April	5738.63	6729.2

The LOTOS-EUROS simulations showed that on April 15, 2010 at 00:00 (UTC), (Figure 4(a)) wind patterns advected the modeled ash cloud in South-East direction toward continental North-West Europe. This closely matches the WRF-Chem simulation also from 00:00 (UTC) April 15 (Figure 4(c)). This is South-East advection of the ash cloud during April 15, 2010 and until April 17, 2010 at 00:00 (UTC) (Figure 4(b)), when the modeled ash cloud is advected toward continental Europe. The LOTOS-EUROS model simulation also shows a good match to the VAAC volcanic ash advisory (VAA) generated operationally at the time of the eruption. The VAA's (Figure 4(e) and 4(f)) showed ash being forecasted across continental Europe as well as from surface to FL200 (approximately 6 km above sea level as flight levels are on a pressure based coordinate system) ash across the United Kingdom (Figure 4(e)). These similarities among different model simulations are from the similar ESP definitions and also possibly from the same or similar wind fields driving data. Table 3 is the comparison of the total mass calculated from LOTOS-EUROS model and WRF-Chem model. Although the values from two models are not same, they are of same magnitude and not different

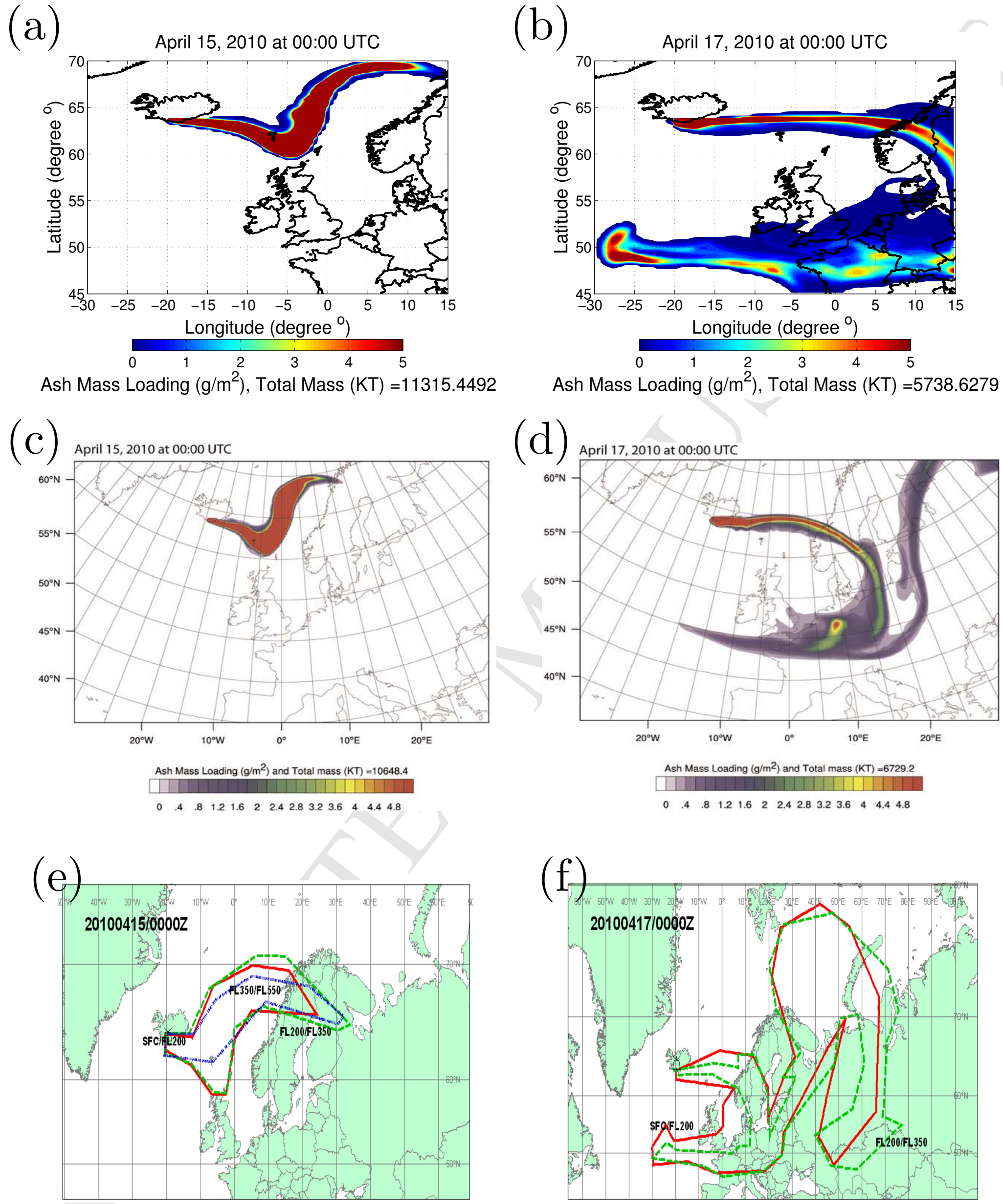

Figure 4: Volcanic ash simulations with different models (a)(b) LOTOS-EUROS, (c)(d) WRF-Chem and (e)(f) NAME at two time snapshot (a)(c)(e) 00:00 (UTC) April 15 and (b)(d)(f) 00:00 (UTC) on April 17, 2010.

too much, which means the LOTOS-EUROS model can produce reasonable simulation results as WRF-Chem does. Note that the differences might be caused by the difference in simulation of two models such as advection scheme, deposition scheme, etc.

Figure 5 is the decomposition of Figure 4(b) with different ash bins defined in Table 1. From Figure 5, we can see the coarse bins vash_1 and vash_2 only remain in the plume near the source, which is because of processes of sedimentation and deposition. In contrast, fine ash bins from vash_3 to vash_6 (particles finer than 63 μm) are transported along the plume to continental Europe. This result fits the fact that after several days in continental Europe only finer ash bins were detected (Webley et al., 2012), so that LOTOS-EUROS simulation can be considered as realistic. It shows to us that along the plume only these finer ash bins are those which can be measured. Comparison of the total mass from the LOTOS-EUROS model with the full extent of all three levels in the VAA and the total mass from WRF-Chem, show that the LOTOS-EUROS model matches well to the NAME model and WRF-Chem model simulations.

As shown above, LOTOS-EUROS model is capable of modeling volcanic ash transport problem. Table 3 implies that different VATDMs will provide different forecast values because different models have different details, therefore only relying on VATDM to make forecast is not sufficient, that is also one of the motivations for using assimilation to correct VATDM to improve the forecast accuracy. In the following, a data assimilation technique will be introduced and used to combine LOTOS-EUROS model and measurement information to improve the ash transport forecast accuracy.

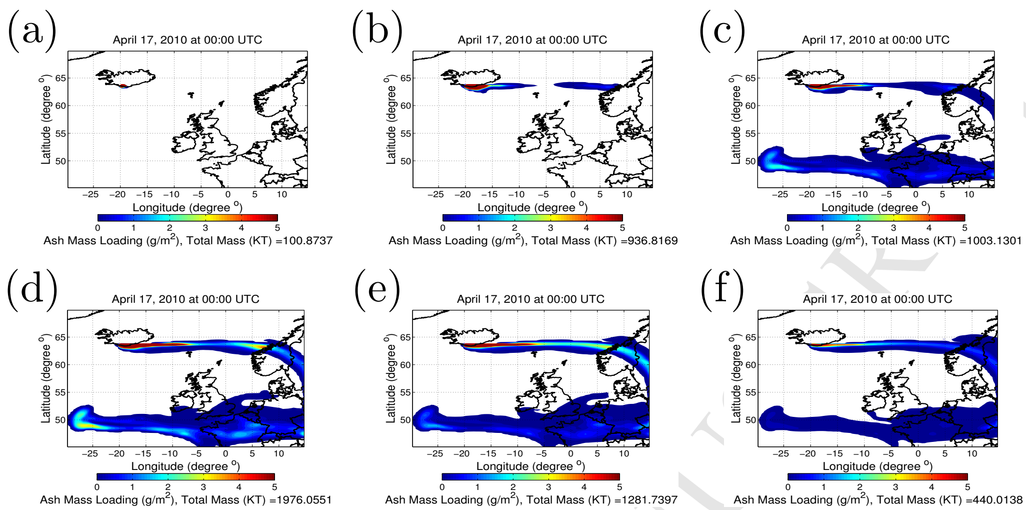

Figure 5: LOTOS-EUROS simulation with different bins. (a) vash_1, (b) vash_2, (c) vash_3, (d) vash_4, (e) vash_5 and (f) vash_6.

4. Aircraft-based Measurements

4.1. Measurements description

During the period of eruption of the Icelandic volcano Eyjafjallajökull, a large number of different scientific measurement campaigns were performed to gather information about the nature and occurrence of the ash plume. The measurements comprised for example LIDAR measurements (Pappalardo et al., 2010; Tesche et al., 2010; Groß et al., 2010; Miffre et al., 2010; Flentje et al., 2010), satellite observations (Stohl et al., 2011), groundbased in-situ measurements (Schäfer et al., 2010; Emeis et al., 2011), as well as balloon (Flentje et al., 2010) and aircraft based measurements (Weber et al., 2010; Schumann et al., 2011; Bukowiecki et al., 2011; Eliasson et al., 2011; Lolli et al., 2010). Aircraft-based measurements are of special interest, because they allow sampling of the ash plume with a high temporal and spatial resolution. Another beneficial aspect of aircraft measurements is that they are more flexible than other type measurements, because usually the aircraft is operated as a "state aircraft" enabling operations in otherwise closed air space where the pilots are able to change the flight plan in-flight in direct contact with air traffic control or wisely decide to follow the downwind ash trend to obtain the best observations.

During the period of that eruption, the outskirts of the eruption plume were entered directly by research flights (Figure 6(a)), delivering most direct measurements within the eruption plume during this eruptive event. All of the measurement flights were equipped with optical particle counters for in-situ measurements. Real-time monitoring of the particle concentrations was possible during the flights and In-situ measurements from the eruption plume were obtained with high time- and spatial-resolution. It has been proven that by entering the outskirts of the plume directly the research aircraft can detect ash concentrations of up to 2000 μg m^{-3} (Weber et al., 2012). That used to be considered as the highest concentration an aircraft can endure at that time, because areas with ash concentration higher than 2000 μg m^{-3} were classified as No Fly Zone (NFZ) (Zehner, 2010), which means the aircraft flying in these areas can crash. However, recently 2000-4000 μg m^{-3} is classified as medium level concentration (EASA, 2011). Many airlines are certified to operate in this regime based on the application of Safety Risk Assessment. Therefore now the highest concentration an aircraft can endure is updated to be 4000 μg m^{-3} instead of 2000 μg m^{-3}.

Optical particle counters (OPC) were used for in-situ ash concentration measurements. The principle of OPC's can be summarized as follows: Ash

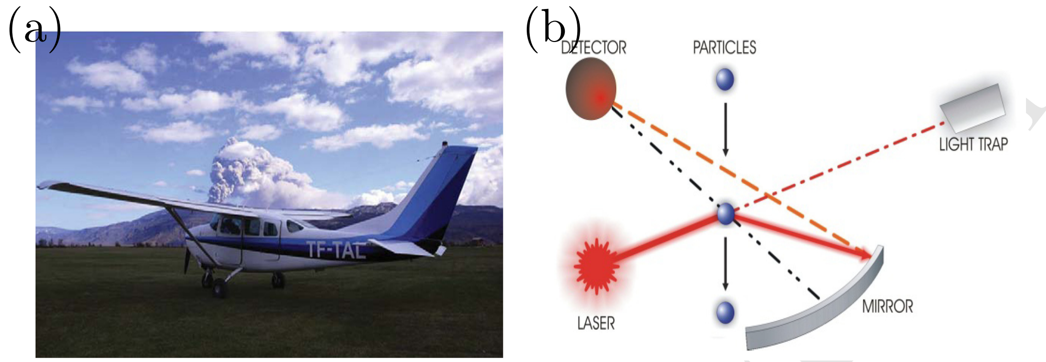

Figure 6: (a) Example of aircrafts used for volcanic ash measurements and (b) optical particle counter OPC equipped on aircrafts. Courtecy from (Weber et al., 2012) and (Weber et al., 2010), respectively.

contaminated air is pumped through the OPC where the particles cross a continuous laser beam. Every single particle causes a scattering/diffraction of the laser beam. This is recorded by a detector that counts the particles, see Figure 6(b). Moreover, scattering/diffraction intensity of the laser beam is a measure for the size of the particles. From that, the mass can be calculated, provided the density of the particles is known. A mean mass density of 2.65 gcm^{-3} (Heim et al., 2008) for the coarse mode ash particles is recommended to use by European Facility for Airborne Research (EUFAR) for Eyjafjallajökull volcano ash.

In our study, the most interesting thing is how accurate OPC's measurements are, because the knowledge of uncertainties is crucial for a successful data assimilation. Through a direct laboratory calibration experiment, in which the mass concentration obtained with the OPC was compared with the absolute mass concentration gathered on a gravimetric filter, the deviation between the gravimetric measurement and the OPC was about 10%

(Weber et al., 2010) which can be taken as the instrumental error for this type of measurements in well calibrated cases.

4.2. Model representation error

For assimilation of measurements with a simulation model, it is necessary to quantify the model representation error. The model representation error is the difference between the quantity that instrument tries to observe, and what the model could represent in terms of its state. This does not include instrumental errors as defined above, or model deficiencies such as inaccurate input parameters, but only the difference due the model being defined on a discrete grid with finite resolution and simulations valid for discrete time steps.

As shown in Section 2, the spatial resolution of the model used in this paper is around 25 km $\times$ 25 km $\times$ 1 km, therefore the volume of one grid-box is about 625 km^3. Through model processing, the concentration of one grid-box represents an average value for this grid-box, while one aircraft-based measurement is a sample (a point value) in a 3 dimensional field. In this paper, we choose the in-situ measurement corresponding to the grid-box average value. This approximation makes sense only when two assimilated measurements are positioned in two different grid-boxes. This requires that the assimilation frequency is not too high, so that the measurements used in two sequential assimilation steps are in different grid-boxes. Moreover, the assimilation frequency should also not be too low because a measuring aircraft usually can work in the sky for less than 10 hours continuously (Weber et al., 2012; Schumann et al., 2011). If an hourly assimilation frequency is chosen, then along the whole route, only less than 10 measurements will be used, which is a waste for other continuous measurements. Therefore based on the analysis above and also considering the aircraft speed of 100-200 km/h (Weber et al., 2012) and the LOTOS-EUROS horizontal resolution, a 15 minutes assimilation frequency is chosen in this study. Within 15 minutes, the aircraft can fly over about 2 grid-boxes in the model, which guarantees different assimilated measurements are in different grid-boxes. The model time step cannot be over the assimilation time step, hence in this paper, 15 minutes is also chosen to be one model time step, without loss of generality. Note that if the research aircraft is faster or the horizontal resolution is higher, the assimilation frequency can be chosen smaller than 15 minutes (e.g., 10 or 5 minutes which can be considered sufficient).

Through the settings defined above, the observation almost corresponds to one model state in a grid-box, which means the representation error of the model is probably small. For the moment we will there not explicitly specify a model representation error, but implicitly assume that it is zero. Therefore, the total observation representation error, defined as the sum of the instrumental error and the model representation error, is taken as 10% in this paper.

Since the knowledge about the uncertainties and representation errors of aircraft measurements are known, data assimilation can now be used to combine observations with the model to get an improved estimate of the ash load.

5. Sequential data assimilation methodology

5.1. Stochastic state space representation

For application of the filter algorithm to the LOTOS-EUROS model, a stochastic representation must be defined for the model error. The specification of uncertainties is crucial for a successful data assimilation. Using a stochastic model for several uncertain parameters, an assimilation scheme is able to produce an optimal estimate of the state and parameters given the observations. For application of the filter algorithms to a dynamical model, a stochastic representation should be written in a state-space form according to:

$$x(k) = M_{k-1}(x(k-1)) + w(k-1), \quad w(k-1) \sim N(0, Q(k-1)) \tag{3}$$

The state-space operator M_{k-1} describes the time evolution from the time $k-1$ to k of the state vector x. In this paper, x contains the ash concentrations in the model grid boxes for the 6 size modes as described in Section 2. The random forcing term w is drawn from the normal distribution with zero mean and covariance matrix Q. The definitions of w and Q will be different per experiment, and are discussed in detail in the coming sections.

5.2. Observational operator

The state of the observational network is defined by the observation operator H that maps state vector x to observation space y:

$$y(k) = H_k(x(k)) + v(k), \quad v(k) \sim N(0, R), \tag{4}$$

where the observation representation error v is drawn from Gaussian distribution with mean 0 and covariance matrix R. This error accounts for the instrumental error as well as for the model representation error (Section 4.2). With the later assumed to be zero, the value of v is solely the instrumental error, which has been estimated to be 10% of the measured values y.

Here, y contains aircraft in-situ concentration, the states are updated every time step of 15 minutes (see Section 4.2) given the new instantaneous concentration. The operator H then simply selects the grid cell in x that corresponds to the observation location. In this paper, for the purpose of investigating the performance of aircraft-based measurements in data assimilation system, only one aircraft is considered to provide measurements. In this scenario, at a fixed time only one measurement is obtained and the observation location keeps changing with the time because aircraft is movable.

5.3. ***Ensemble Kalman Filter***

The assimilation technique used in this study is an Ensemble Kalman Filter technique (EnKF). Apart from the original formulation in (Evensen, 1994), other formulations have been introduced such as the Ensemble Kalman Smoother (EnKS) (Evensen and van Leeuwen, 2000), Ensemble Square Root Filter (EnSR) (Evensen, 2004), Reduced Rank Square Root Filter (RRSQRT) (Verlaan and Heemink, 1997), etc. Ensemble-based assimilation is easy to implement, suitable for real-time estimation of concentrations and allows a very general statistical description as Eq. (3). Different methods have different advantages and disadvantages. This paper aims to compare the performance of aircraft-based measurements in data assimilation systems, not to compare performance of different data assimilation schemes. Therefore, in this paper, we choose the commonly used method EnKF in our data assimilation system.

The EnKF essentially is a Monte Carlo sequential method (Evensen, 2003), based on the representation of the probability density of the state estimate in an ensemble of N states, $\xi_1, \xi_2, \cdots, \xi_N$. Each ensemble member is assumed to be a single sample out of a distribution of the true state.

In the first step of this algorithm an ensemble of N states $\xi^a(0)$ is generated to represent the uncertainty in $x(0)$. In the second step, the *forecast* step, the stochastic model propagates the ensemble members from the time $k-1$ to k:

$$\xi_j^f(k) = \tilde{M}_{k-1}(\xi_j^a(k-1)) + Gw_j(k-1), \tag{5}$$

when w_j represents the realizations of a white noise process w. The filter state is a stochastic distribution with mean x^f and covariance P^f following:

$$x^f(k) = \frac{1}{N}\sum_{j=1}^{N} \xi_j^f(k). \tag{6}$$

$$L^f(k) = [\xi_1^f(k) - x^f(k), \cdots, \xi_q^f(k) - x^f(k)], \tag{7}$$

$$P^f(k) = \frac{1}{N-1} L^f(k) L^f(k)'. \tag{8}$$

When measurements become available, the ensemble members are updated in the *analysis* step using the Kalman gain:

$$K(k) = P^f(k)H(k)'[H(k)P^f(k)H(k)' + R]^{-1}, \tag{9}$$

$$\xi_j^a(k) = \xi_j^f(k) + K(k)[y(k) - H(k)\xi_j^f(k) + v_j(k)], \tag{10}$$

where v_j represents realizations of the observation representation error v.

Advantages of the ensemble formulation is that the dynamical model is not restricted to linearity and the implementation can be rather simple. The number of required ensemble members depends on the complexity of the probability density function (eps) to be captured, which is usually determined by the nonlinearity of the model and the description of the involved uncertainties. In general, an ensemble with 30–100 members is acceptable to keep computations feasible (Barbu et al., 2009).

6. Assimilation results and discussions

6.1. *Experimental setup*

The EnKF is applied to the stochastic version of LOTOS-EUROS. The study comprises experiments with different settings for the uncertainty in parameters such as plume height (PH), mass eruption rate (MER), particle size distribution (PSD) and vertical mass distribution (VMD). In this paper, the uncertainty of PH and MER are taken as 20 % and 50 %, respectively (see Section 2). The stochastic version of the model is built by considering these two uncertain parameters. The temporal correlation for a uncertain model parameter defines how the value at current time is related to that at prior time. However, due to volcano inner fierce and fast physical processes, the PH and MER could change very fast, and therefore taking temporal correlation into account is not necessary and realistic. Therefore, in this paper, we consider PH and MER as temporal uncorrelated. Aircraft-based measurements are used in the analysis step of the EnKF algorithm; the uncertainty in the measurements has been investigated as a fixed standard deviation of 10 %, see Section 4. This paper focuses on studying how aircraft-based measurement performs well in a data assimilation system, thus it is not necessary to use real measurements. Therefore, the measurements in

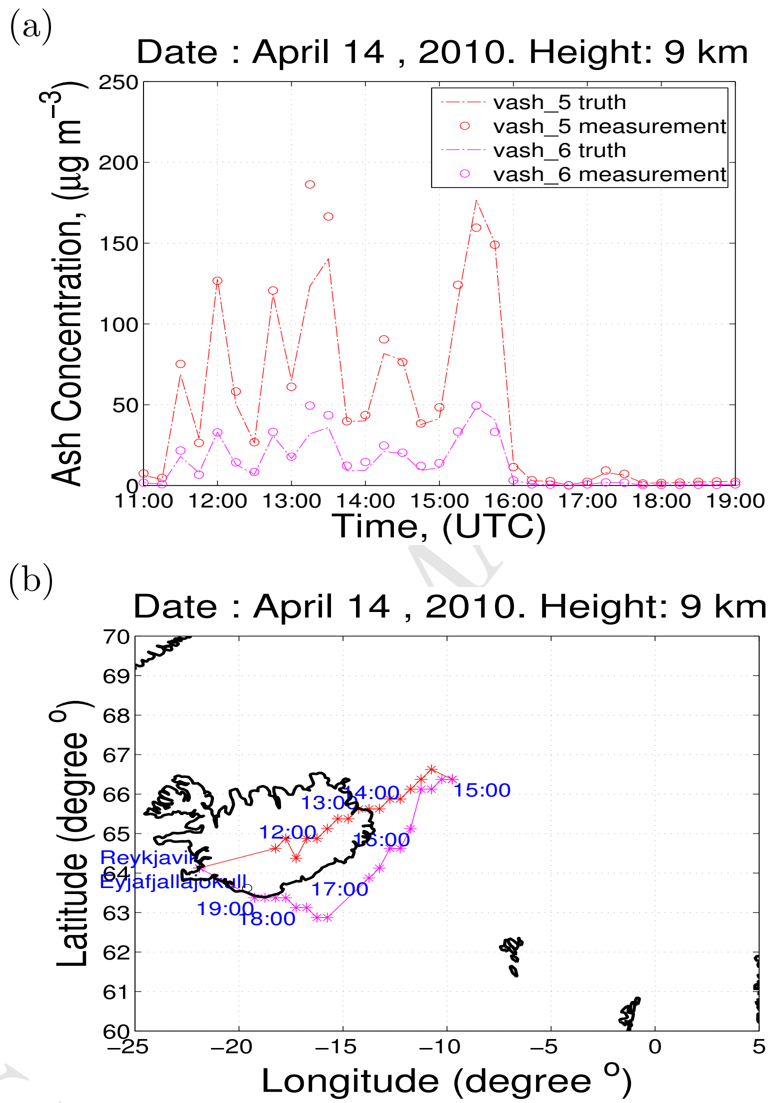

Figure 7: (a) Aircraft-based Measurements for vash_5 and vash_6. (b) is the designed route at 9 km where the measuring aircraft enters the outskirts of ash plume, red and magenta lines represent different flying directions to Reykjavik airport.

this paper are designed based on the real aircraft-based measuring campaigns (Weber et al., 2012). In these campaigns, concentrations of ash with diameter 0 to 2.5 and 2.5 to 10 μm were observed, which from Table 1 respectively corresponds to vash_5 and vash_6 in this paper.

From (Weber et al., 2012; Schumann et al., 2011), a measuring aircraft can work in the sky for less than 10 hours continuously, so based on this condition, a 10 hour aircraft measurement experiment is designed. Note that in reality usually an aircraft measurement mission is 4 to 6 hours, 10 hours is not very realistic, but we use the duration of 10 hours in our twin experiments to evaluate effect of assimilation over a longer time. The height of interest in this paper is 9 km as mentioned in Section 1. The flight routes are chosen at an altitude of 9 km, 7 km, 5 km, 3 km separately to study which level measurements provide the best air traffic advisory for 9 km. The start time of Eyjafjallajökull eruption is set at 9:00 (UTC), 14 April 2010, and the aircraft-based measurements are designed to start at 11:00 (UTC), 14 April 2010. The whole assimilation time is from 11:00 to 19:00 (UTC), 14 April 2010. The flying route is designed as shown in Figure 7(c) based on the fact that the measuring aircraft can enter the plume outskirt where the ash concentration is less than 4000 μg m^{-3} (see Section 4.1). During this period, measurements are taken every 15 minutes, see Figure 7(a) and Figure 7(b) taken at 9 km for example.

From the start time to aircraft returning time, the simulation parameters are set as introduced in Section 2. For evaluating the performance of assimilation, twin experiments are designed with the Truth obtained as one realization of the stochastic model by adding uncertainty 20 %, 50 % to PH, MER, separately. The measurements are obtained through combining the Truth values with 10 % uncertainty, see Figure 7(a) and Figure 7(b).

Table 4: Plume height and Eruption rate used in LOTOS-EUROS to generate the Truth for April 14-18, 2010.

Start Time – End Time	Height ASL (km)	Eruption Rate (kg/s)
4/14 09:00 – 4/14 11:00	8.8	5.23E+05
4/14 11:00 – 4/14 13:00	9.3	5.85E+05
4/14 13:00 – 4/14 15:00	7.8	3.98E+05
4/14 15:00 – 4/14 17:00	9.1	5.38E+05
4/14 17:00 – 4/14 19:00	8.5	4.41E+05
4/14 19:00 – 4/14 22:00	6.3	5.73E+04
4/14 22:00 – 4/15 01:00	4.8	3.13E+04
4/15 01:00 – 4/15 04:00	5.9	4.97E+04
4/15 04:00 – 4/15 17:00	5.0	5.07E+04
4/15 17:00 – 4/16 06:00	7.1	8.32E+04
4/16 06:00 – 4/16 19:00	6.8	8.15E+04
4/16 19:00 – 4/17 01:00	9.2	5.10E+05
4/17 01:00 – 4/17 07:00	8.0	3.12E+05
4/17 07:00 – 4/17 13:00	9.4	3.89E+05
4/17 13:00 – 4/17 19:00	7.9	2.97E+05
4/17 19:00 – 4/18 01:00	8.5	3.93E+05

The experiment procedure can be briefly summarized by stating that the model run starts at 09:00 (UTC), 14 April, 2010 by considering the first initial condition as zero. With the model propagating, the model result from previous time step is taken as the initial condition for the next time step. When the model run arrives at 11:00 (UTC), 14 April, the initial condition gets continuously modified by the data assimilation process through combining all the aircraft-based measurements until the time 19:00 (UTC), 14 April. Thus at this time, an analyzed state (which can be taken as an initial condition for next model run) combining all aircraft measurements of 8 hours can be obtained. Evaluation on this analyzed state will be given to investigate the possible improvement compared to simulation without assimilation. In the remainder of the paper, AnaSta and SimSta are used to denote the analyzed state (obtained with assimilation) and the simulation state (obtained without assimilation), respectively. Thus, $\text{AnaSta}_{19:00(14)}$ denotes AnaSta at 19:00 (UTC), 14 April, 2010 and will be further used to forecast over multiple days (typically one or two days according to NAME model forecast).

6.2. ***Assimilation experiments***

Based on the setup above, an experiment is designed to test whether the analyzed state $\text{AnaSta}_{19:00(14)}$ is improved through an 8 hours continuous assimilation of aircraft-based measurements. For this experiment, the measuring aircraft flies at the 9 km height and the ensemble size is chosen to be 50 in the EnKF system. Before we show the result of $\text{AnaSta}_{19:00(14)}$, first how data assimilation continuously works in this system is explained using Figure 8 and Figure 9.

Figure 8 is the result of specific measurements at one location on 12:00 (UTC), 14 April, 2010. At this time, we can see from Figure 7, the measuring aircraft location is (11.75°W, 65.625°N, 9 km). In Figure 8, the forecast of the ash concentrations at this location in each of the 50 ensemble members shown. The concentrations are distributed around the mean values (96.38 μg m^{-3} for vash_5, 24.80 μg m^{-3} for vash_6) indicated by the black circle. At this time, the measurements of the concentrations are (126.69 μg m^{-3}, 32.93 μg m^{-3}) which is significantly different from the forecast mean. Through assimilating these measurements at this time, analysis values of vash_5 and vash_6 are obtained as (123.61 μg m^{-3}, 32.54 μg m^{-3}) which are much closer to the truth (135.88 μg m^{-3}, 33.88 μg m^{-3}) than the forecast mean. This result illustrates that the assimilated state better approximates the truth than that without assimilation. Moreover, spread in the analysis ensemble is smaller than that of the forecast ensemble, that means the error variance of analysis value is reduced through assimilation.

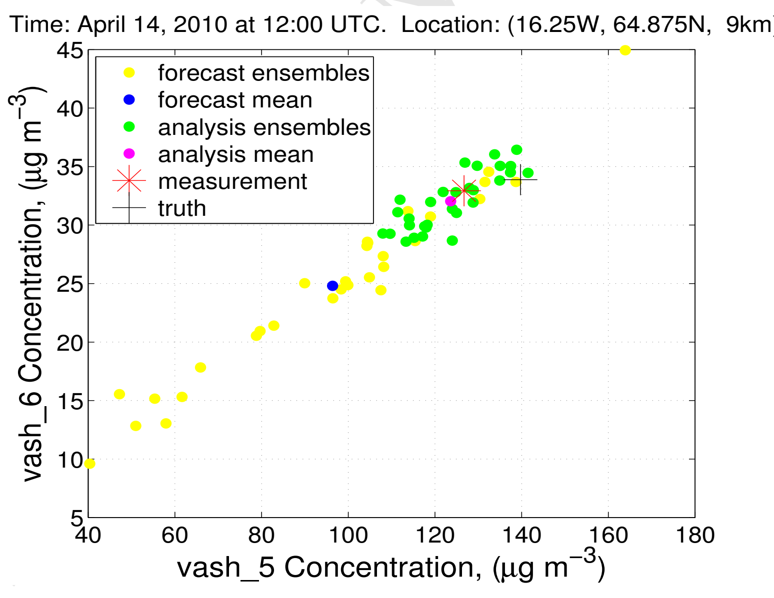

Figure 8: Assimilation at one location.

Figure 8 only shows the assimilation result at the measuring location, we cannot see the influence of the assimilation on the whole plume. It is not clear whether measurements from one location can influence the whole plume or not. Figure 9 is used to answer this question. In Figure 9, without loss of generality the time 16:30 (UTC), 14 April, 2010 is chosen to show the result for the whole plume at 9 km. $\mathrm{Tru}_{16:30(14)}$ in Figure 9 is the truth state, while $\mathrm{FC}_{16:30(14)}$ is the forecast state and $\mathrm{AnaSta}_{16:30(14)}$ is the analyzed state. By comparing $\mathrm{FC}_{16:30(14)}$ with $\mathrm{AnaSta}_{16:30(14)}$, we can see that with assimilating aircraft-based measurements at one location, the difference between them only appears in a local area (approximatly the red ellipse in Figure 9) around the measuring location, while the results outside this local area are hardly changed. This means that the assimilation process doesn't influence the entire plume, but only a local area around the measuring aircraft location. Note that this is achieved without explicit enforcing of localization as for example in (Houtekamer and Mitchell, 1998). In the chosen setup without temporal correlation (see Section 6.1), the ensembles consist of patterns that arise from uncertainties during a single time step. The spatial impact of observations from a single location is therefore bounded to an area where ashes present have been emitted during a short period. Moreover, in this local area, $\mathrm{AnaSta}_{16:30(14)}$ is much closer to $\mathrm{Tru}_{16:30(14)}$ than $\mathrm{FC}_{16:30(14)}$. This shows that through each assimilation, the state within a local area is improved. Therefore with a continuously assimilation using aircraft-based measurements of changing locations, the states in a large area around the measuring flight route will be improved, as shown in Figure 7(c).

Next, the experiment result of $\mathrm{AnaSta}_{19:00(14)}$ is shown in Figure 10. $\mathrm{Tru}_{19:00(14)}$ is the Truth at 19:00 (UTC), 14 April, 2010 which is imple-

(a) (b) (c)

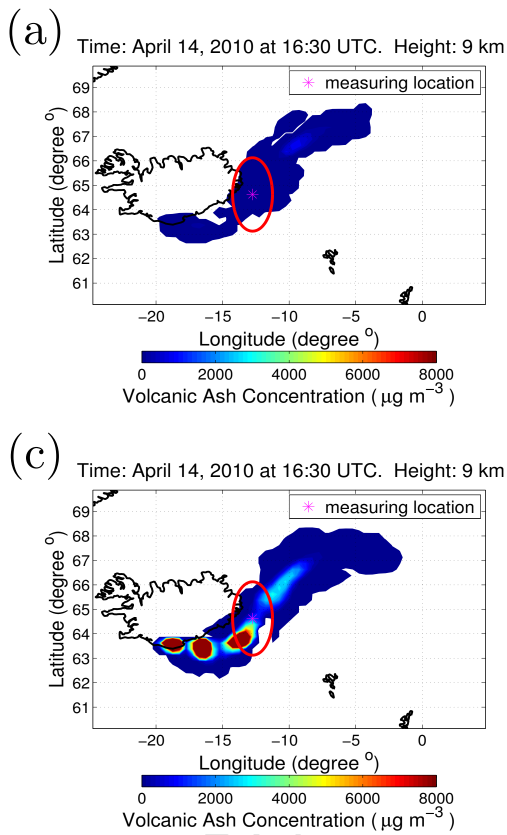

Figure 9: Assimilation results during continuously assimilation (red ellipse represents a local area where the assimilation can influence). (a) $\mathrm{Tru}_{16:30(14)}$, (b) $\mathrm{FC}_{16:30(14)}$ and (c) $\mathrm{AnaSta}_{16:30(14)}$.

mented based on Table 4. $\mathrm{SimSta}_{19:00(14)}$ is the simulation result directly implemented based on input parameters specified in Table 2 without assimilating aircraft-based measurements. $\mathrm{AnaSta}_{19:00(14)}$ is the assimilation result at this time with assimilating aircraft-based measurements (detailed settings are in Section 6.1). Big differences can be observed between Figure 10(a) and Figure 10(b). The difference is caused by implementing with different PH and MER. In reality, $\mathrm{Tru}_{19:00(14)}$ is unknown, thus $\mathrm{SimSta}_{19:00(14)}$ is used as the initial condition for the forecast over multiple days. $\mathrm{AnaSta}_{19:00(14)}$ is that with continuously assimilating aircraft-based measurements. Comparing $\mathrm{AnaSta}_{19:00(14)}$ and $\mathrm{SimSta}_{19:00(14)}$, we can see both of them overestimate the truth, but $\mathrm{AnaSta}_{19:00(14)}$ is much closer to $\mathrm{Tru}_{19:00(14)}$ and the overestimation is much lower than $\mathrm{SimSta}_{19:00(14)}$. This means the state after assimilating aircraft-based measurements is much more accurate than that without assimilation.

Now we have verified that through continuously assimilating aircraft-based measurements, an improved state is obtained. There are two main reasons that explain why it performs very well: (a) The measuring aircraft always follows the ash flowing trend and enters the plume outskirt to measure concentration. This movable aircraft-based measuring path makes the measurements always informative and useful for data assimilation; (b) the uncertainty knowledge of PH, MER and the measurements is known, which is important for EnKF to generate proper ensembles.

$\mathrm{AnaSta}_{19:00(14)}$ can be used as an initial condition to do forecast over multiple days to see the possible improvement in advisories to aviation. Without loss of generality, the forecast at 00:00 (UTC) 15 April is chosen as illustra-

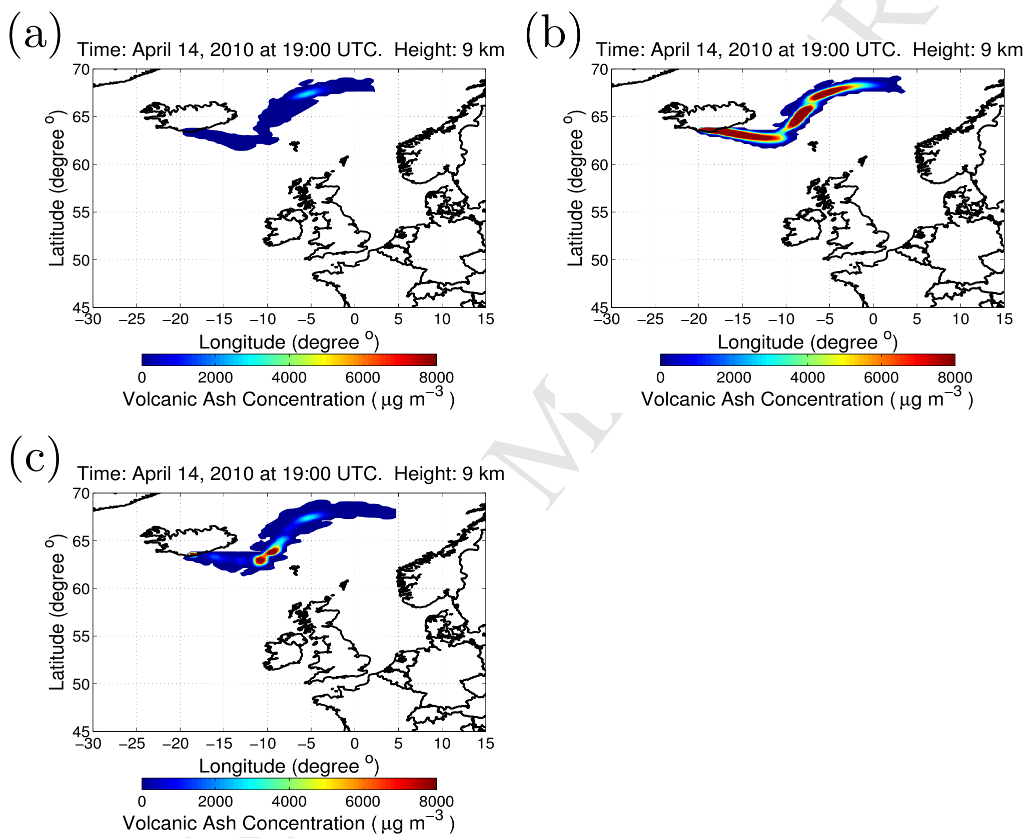

Figure 10: Comparison of results with and without assimilating aircraft-based measurements. (a) $\mathrm{Tru}_{19:00(14)}$, (b) $\mathrm{SimSta}_{19:00(14)}$ and (c) $\mathrm{AnaSta}_{19:00(14)}$.

tion in Figure 11. $\mathrm{FC}^{n}_{00:00(15)}$ and $\mathrm{FC}^{a}_{00:00(15)}$ are used to represent the forecast initiated with $\mathrm{SimSta}_{19:00(14)}$ and the forecast with $\mathrm{AnaSta}_{19:00(14)}$ as an initial condition.

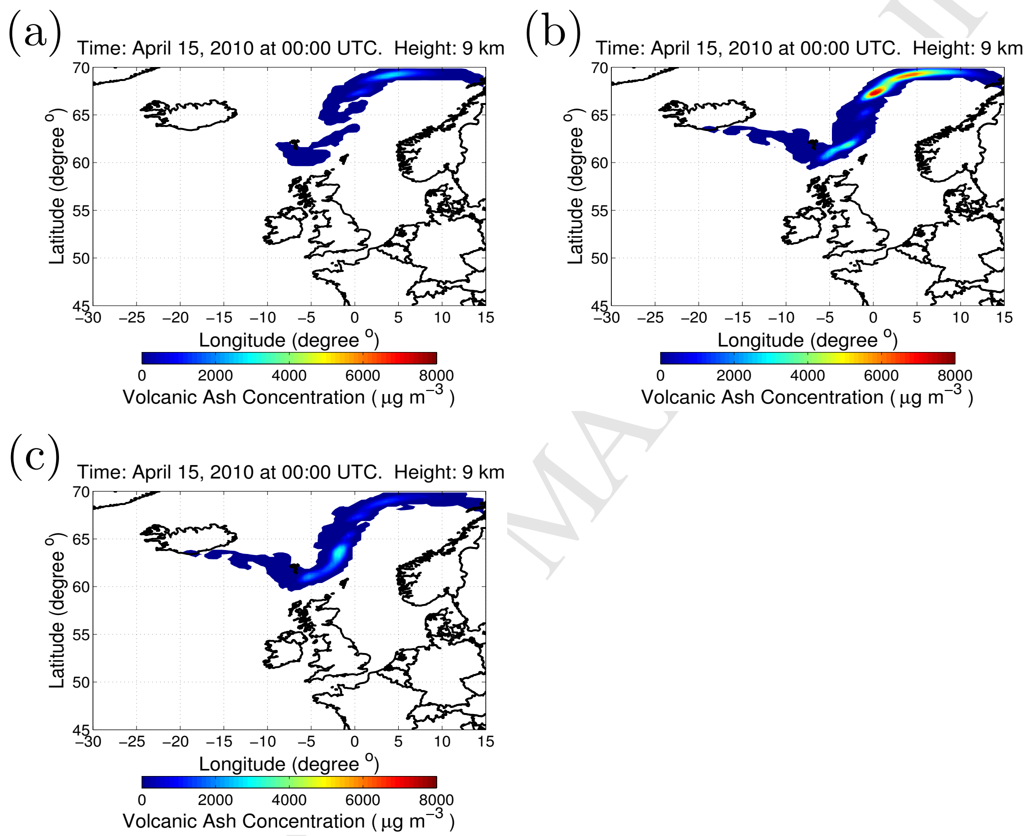

Figure 11: Comparison of Volcanic Ash Forecast with assimilating aircraft-based measurements and without assimilation. (a) $\mathrm{Tru}_{00:00(15)}$, (b) $\mathrm{FC}^{n}_{00:00(15)}$ and (c) $\mathrm{FC}^{a}_{00:00(15)}$.

In Figure 11, at time 00:00 (UTC) 15 April, 2010, we can see $\mathrm{FC}^{a}_{00:00(15)}$ better approximates $\mathrm{Tru}_{00:00(15)}$ than $\mathrm{FC}^{n}_{00:00(15)}$. The result shows the forecast accuracy is improved through assimilating aircraft-based measurements. Note that in Figure 11(a), the plume does not appear south of Iceland, it means in this area the ash plume is below the altitude of 9 km. In real life, the truth is unknown, thus usually Figure 11(b) is used to provide advice to decision makers. In this experiment, if we use $\mathrm{FC}^{n}_{00:00(15)}$ for the advice, then it will be that at 9 km ash concentrations in West-North areas outside Norway are higher than 6000 μg m^{-3}. Whereas in fact this advice is inaccurate compared to the truth which shows in these areas ash concentrations are lower than 4000 μg m^{-3}. This clearly shows only using simulation to provide advice is not sufficient for decision makers. Figure 11(c) is the assimilation forecast combining 8 hours continuous aircraft real-time measurements (Figure 7). The only difference between Figure 11(c) and Figure 11(b) is that Figure 11(c) assimilates aircraft-based measurements. From Figure 11(c), we can get an accurate advice with a much closer to truth estimate at 00:00 (UTC) 15 April, where ash concentrations in all the areas at 9 km are lower than 4000 μg m^{-3}. This is a big improvement compared to Figure 11(b).

In this experiment, through initiation with $\mathrm{AnaSta}_{19:00(14)}$, the forecast of volcanic ash transport has been significantly improved. This tells us for volcanic ash forecast, with a good state obtained from assimilating aircraft-based measurements, it can provide an improved advice for aviation. In the following, two other experiments are designed to study (1) for the interested advice at height level of 9 km, at which altitude the aircraft should fly to give the best analyzed state $\mathrm{AnaSta}_{19:00(14)}$? (2) how important is having a good knowledge of uncertainties in parameters PH, MER and measurement?

6.3. ***Experiments with Different Flight Levels***

In this experiment, measurements are simulated at different altitudes as 7 km, 5 km, 3 km, respectively. The interested level is still 9 km as in last experiments and Figure 12(a), Figure 12(b) and Figure 12(c) are the designed aircraft measurement routes at different heights 3 km, 5 km, 7 km, respectively. The performance of assimilating these measurements compared with the 9 km measurements is shown in Figure 13. We extend $\text{AnaSta}_{19:00(14)}$ to $\text{AnaSta}^3_{19:00(14)}$, $\text{AnaSta}^5_{19:00(14)}$, $\text{AnaSta}^7_{19:00(14)}$ and $\text{AnaSta}^9_{19:00(14)}$ to represent the analyzed state at 19:00 (UTC) 14 April, 2010 through assimilating aircraft-based measurements from heights 3 km, 5 km, 7 km and 9 km, respectively. $\text{Tru}_{19:00(14)}$ is the truth and $\text{SimSta}_{19:00(14)}$ is the simulation result without assimilation. From Figure 13(c) to Figure 13(f), we can see that all cases with different altitude perform worse than the 9 km case, and some of them (3 km case and 5 km case) are even worse than the case without assimilation.

From these comparison, we can get that the locations (flight levels in this paper) of aircraft-based measurements are crucial for providing a more accurate analyzed state on interested level. The best $\text{AnaSta}_{19:00(14)}$ is that assimilating aircraft-based measurements from the same flight level with interested level. Furthermore, Figure 13(e) is also shown to perform an improvement compared to the case without assimilation. Thus based on $\text{AnaSta}^7_{19:00(14)}$ we can also obtain an improved advice where the overestimation of ash concentrations has been reduced compared to $\text{SimSta}_{19:00(14)}$.

Through this experiment, two conclusions can be drawn that (1) in order to get the best analyzed state on the interested commercial aeroplane level with assimilation, the aircraft-based measurements should be preferably taken at the same level of height; (2) If this level measurements can not be provided, through assimilating measurements from close levels, an acceptable analyzed state can still be obtained.

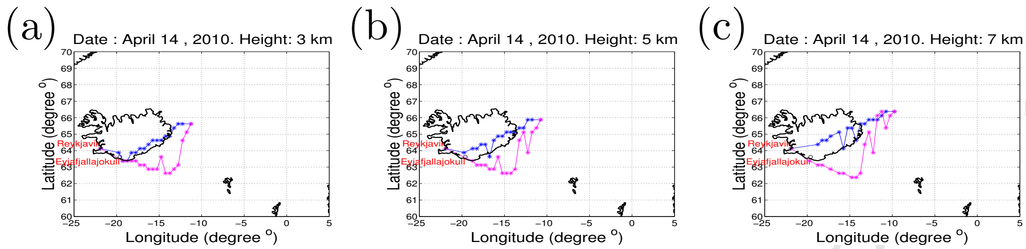

Figure 12: Designed aircraft-based measurements on different flight levels (a) 3 km, (b) 5 km and (c) 7 km.

6.4. Uncertainties in PH, MER and measurement

This experiment is undertaken to investigate the importance of having a good knowledge of uncertainties for assimilating aircraft-based measurements. In this paper, the uncertainties of PH, MER and measurements are considered to be 20 %, 50 % and 10 % respectively as discussed in Section 6.1. However, if the uncertainty information can not be well estimated, how will the assimilation perform? What are the consequences due to overestimation and underestimation of uncertainty? Which uncertainty information is of most importance for ash forecast? To answer these three questions, we modify the three uncertainties in the experiment one by one and evaluate the performance. For evaluating influence of one uncertainty, we change its uncertainty with underestimation and overestimation, separately, while, we keep uncertainties of other two unchanged. The results are summarized in Figure 14.

Figure 14(g) is the truth, Figure 14(h) is the analyzed state through assimilating aircraft-based measurements with the correct uncertainty information of PH, MER and measurement. Figure 14(a) and Figure 14(d) are the results with the wrong PH uncertainty of 10 % and 30 %, respectively.

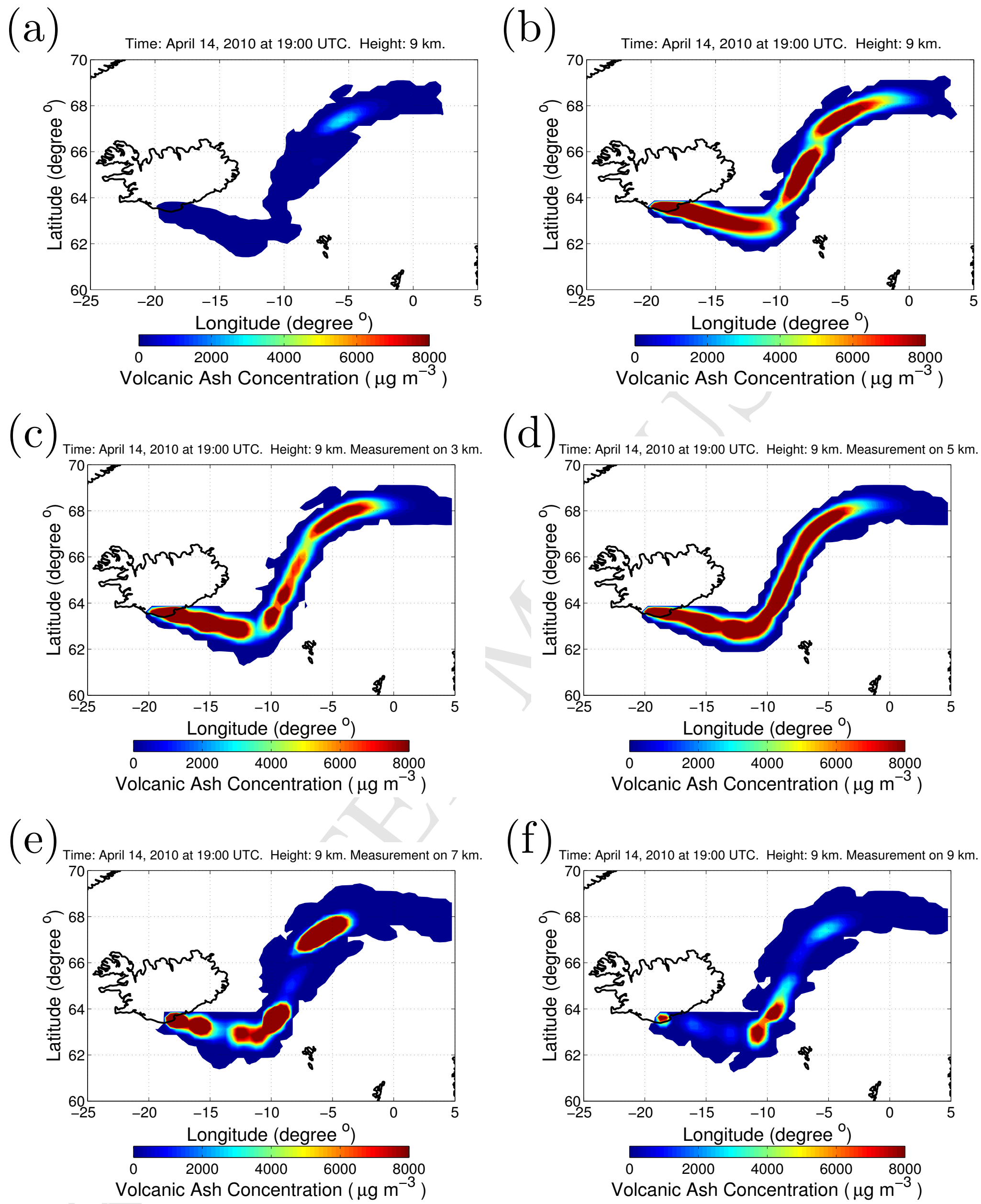

Figure 13: $\text{AnaSta}_{19:00(14)}$ Comparison with assimilating aircraft-based measurements taken from different flight levels. (a) $\text{Tru}_{19:00(14)}$, (b) $\text{SimSta}_{19:00(14)}$, (c) $\text{AnaSta}^{3}_{19:00(14)}$, (d) $\text{AnaSta}^{5}_{19:00(14)}$, (e) $\text{AnaSta}^{7}_{19:00(14)}$ and (f) $\text{AnaSta}^{9}_{19:00(14)}$.

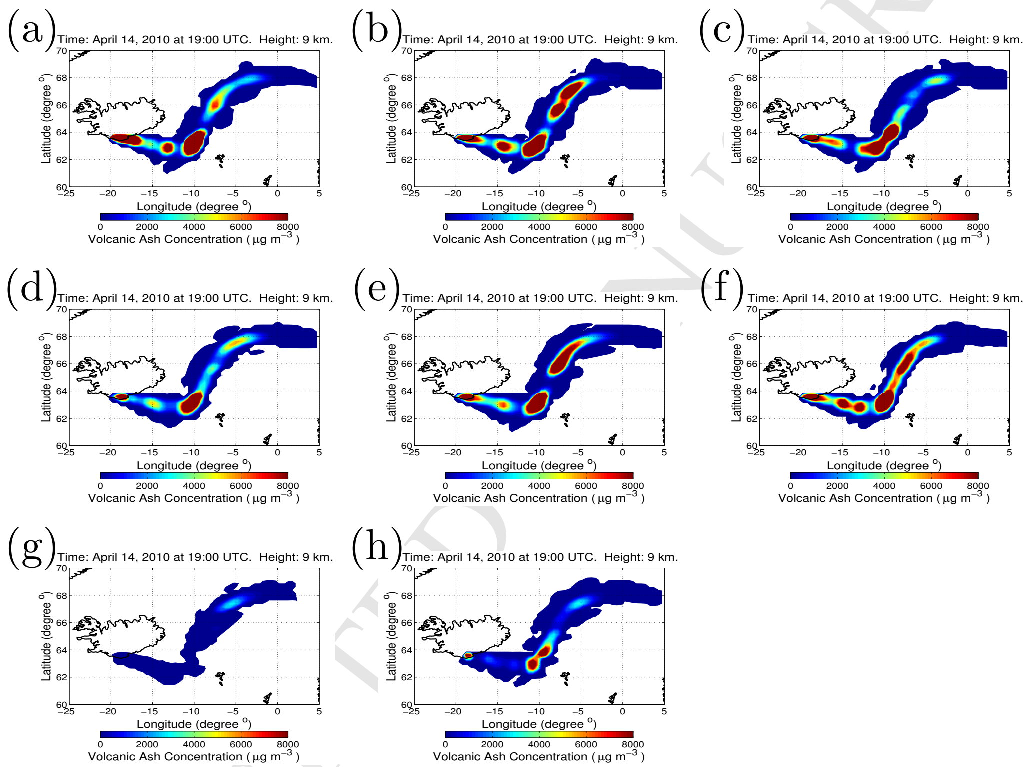

Figure 14: $\mathrm{AnaSta}_{19:00(14)}$ implemented with different uncertainties of PH, MER and measurement. (a) $\mathrm{AnaSta}^{PH10}_{19:00(14)}$, (b) $\mathrm{AnaSta}^{MER30}_{19:00(14)}$, (c) $\mathrm{AnaSta}^{meas01}_{19:00(14)}$, (d) $\mathrm{AnaSta}^{PH30}_{19:00(14)}$, (e) $\mathrm{AnaSta}^{MER70}_{19:00(14)}$, (f) $\mathrm{AnaSta}^{meas30}_{19:00(14)}$, (g) $\mathrm{Tru}_{19:00(14)}$ and (h) $\mathrm{AnaSta}_{19:00(14)}$.

Similarly, Figure 14(b) and Figure 14(e) are results with the wrong MER uncertainty of 30 %, 70 %; Figure 14(c) and Figure 14(f) are results with the wrong measurement uncertainty of 1 % and 30 % respectively. We extend a superscript in $\mathrm{AnaSta}_{19:00(14)}$ as PH10, PH30, MER30, MER70, meas01 and meas30 to represent these different cases, respectively.

The result in Figure 14 shows that $\mathrm{AnaSta}_{19:00(14)}$ with the correct uncertainties has the best performance to approximate the truth. All the other assimilation results are inferior to $\mathrm{AnaSta}_{19:00(14)}$. Among them, some have very strong overestimation such as $\mathrm{AnaSta}_{19:00(14)}^{MER30}$, $\mathrm{AnaSta}_{19:00(14)}^{MER70}$ and $\mathrm{AnaSta}_{19:00(14)}^{meas30}$. Based on these results, the answer to the first question is that when the uncertainty information is not well estimated, the assimilation accuracy cannot be guaranteed. In order to get a better analyzed state in data assimilation systems, the uncertainties of PH, MER and measurement should be obtained as accurate as possible, otherwise analyzed state can become very unacceptable.

The second question is to investigate the consequences due to overestimation and underestimation of uncertainties. Figure 14(a), Figure 14(b) and Figure 14(c) are forecast with underestimated uncertainty of PH, MER and measurement, respectively. Whereas Figure 14(d), Figure 14(e) and Figure 14(f) are the cases with overestimated uncertainties. The result shows for uncertainties of PH or MER, overestimation can provide a better result, while for uncertainties of measurement, underestimation is better. This knowledge is of practical importance because when we are not sure about some parameter uncertainties in real-life assimilation, this investigation can give a guidance for choosing reasonable initial uncertainties.

Finding the most important uncertainty is equal to investigate which one is the most sensitive to forecast accuracy. For this, we first introduce a measure for sensitivity of accuracy, which is defined as:

$$(SenAccu)_p = \frac{|(TotalMass)_p(i) - (TotalMass)_p(j)|}{|(Uncert)_p(i) - (Uncert)_p(j)|}, \tag{11}$$

where p means one of the parameters PH, MER, measurement, i and j means implementations with parameter uncertainties. Moreover, $(TotalMass)_p$ and $(Uncert)_p$ represent total mass and parameter uncertainties corresponding to some parameter p. Using Eq. (11), we can get sensitivities of PH, MER and measurement as: $(SenAccu)_{PH} = 15.74$, $(SenAccu)_{MER} = 12.69$ and $(SenAccu)_{measurement} = 25.52$. So the parameter sensitivity in descending order is measurement, MER and PH. Thus, the most sensitive parameter for assimilation is measurement whose uncertainty is the most important uncertainty for achieving an accurate analyzed state. Therefore, we should be very careful about defining measurement uncertainty, a slight overestimation can already cause a big inaccuracy.

7. Conclusions

In this paper aircraft-based measurements have been assimilated in a sequential data assimilation system to provide volcanic ash transport forecast. The LOTOS-EUROS model has been adapted to model volcanic ash transport. The experimental results show that the LOTOS-EUROS model is capable as a reliable Volcanic Ash Transport and Diffusion Model. Our goals were to improve ash transport forecast accuracy through assimilating aircraft-based measurements, and to study the impact of measurements from different flight heights and the influence of uncertainties in PH, MER and measurements.

Twin experiments were carried out to evaluate the assimilation results. The results showed through assimilating aircraft-based measurements, the forecast of volcanic ash transport can be significantly improved. The accurate advice of aeroplane flying safety was made through the assimilation forecast, whereas the simulation result gave a wrong advice.

Another experiment revealed that for the interested advice level 9 km, the aircraft-based measurements should be taken at this level. However, when at this level measurements can not be provided, through assimilating measurements from close levels, an acceptable advice can still be obtained. Through comparing assimilation result of correct PH, MER and measurement uncertainty with those of wrong uncertainty information, we found that assimilating aircraft-based measurements only can perform well with sufficient knowledge of the statistics of the uncertainties. Otherwise, accurate assimilation results cannot be guaranteed. One thing needs to be mentioned that from this study, we investigated measurement is the most sensitive parameter for our assimilation system, which only means for assimilating aircraft-based measurements, not for all the other assimilation systems such as assimilating satellite measurements. For these assimilation systems, the sensitivity of parameters still needs to be investigated.

In this paper, we applied an off-line approach for model running and simply used meteorological input data as deterministic. Actually these data also contain uncertainties which have an influence on ash cloud transport. In future work, for more accurate ash forecasting, it is better to take also uncertainties of meteorological data like wind speed into account. This paper only used aircraft-based measurements from one aircraft and showed that ash forecasts were significantly improved through this one aircraft setup. we may expect that with more measuring aircrafts the results will be better than with one aircraft if all the aircrafts can enter outskirt of ash plume to get appropriate measurements.

Aircraft-based type of measurements can perform well in data assimilation system. Therefore based on this study, the real aircraft-based data experiment, which is in process, will be in a follow-up paper which also considers to increase the efficiency of the data assimilation system.

8. Acknowledgements

In this paper, OpenDA software (van Velzen and Verlaan, 2007), (van Velzen and Segers, 2010) was used to perform EnKF data assimilation algorithm.

References

Barbu, A. L., Segers, A. J., Schaap, M., Heemink, A. W., Builtjes, P. J. H., Mar. 2009. A multi-component data assimilation experiment directed to sulphur dioxide and sulphate over Europe. Atmospheric Environment 43 (9), 1622–1631.

Bonadonna, C., Costa, A., 2013. Plume height, volume, and classification of explosive volcanic eruptions based on the Weibull function 75 (8), 1–19.

Bonadonna, C., Folch, A., Loughlin, S., Puempel, H., Aug. 2012. Future developments in modelling and monitoring of volcanic ash clouds: outcomes from the first IAVCEI-WMO workshop on Ash Dispersal Forecast and Civil Aviation. Bulletin of Volcanology 74 (1), 1–10.

Bonadonna, C., Webley, P. W., Hort, M. C., Folch, A., Loughlin, S. C., Puempel, H., Feb. 2014. 2nd IUGG-WMO Workshop on Ash Dispersal Forecast and Civil Aviation, Consensual Document.
URL https://vhub.org/resources/add-contribution/3343

Bukowiecki, N., Zieger, P., Weingartner, E., Jurányi, Z., Gysel, M., Neininger, B., Schneider, B., Hueglin, C., Ulrich, A., Wichser, A., Henne, S., Brunner, D., Kaegi, R., Schwikowski, M., Tobler, L., Wienhold, F. G., Engel, I., Buchmann, B., Peter, T., Baltensperger, U., Oct. 2011. Ground-based and airborne in-situ measurements of the eyjafjallajökull volcanic aerosol plume in Switzerland in spring 2010. Atmospheric Chemistry and Physics 11 (19), 10011–10030.

Curier, R. L., Timmermans, R., Calabretta-Jongen, S., Eskes, H., Segers, A., Swart, D., Schaap, M., Dec. 2012. Improving ozone forecasts over Europe by synergistic use of the LOTOS-EUROS chemical transport model and in-situ measurements. Atmospheric Environment 60, 217–226.

Draxler, R. R., Hess, G. D., 1998. An overview of the HYSPLIT_4 modelling system for trajectories, dispersion, and deposition. Australian Meteorological Magazine 47, 295–308.

Durant, A. J., Rose, W. I., Sep. 2009. Sedimentological constraints on hydrometeor-enhanced particle deposition: 1992 Eruptions of Crater Peak, Alaska. Journal of Volcanology and Geothermal Research 186 (1-2), 40–59.

EASA, May 2011. EASA Safety Information Bulletin 2010-17R4.

Eliasson, J., Palsson, A., Weber, K., Jul. 2011. Monitoring ash clouds for aviation. Nature 475 (7357), 455.

Emeis, S., Forkel, R., Junkermann, W., Schäfer, K., Flentje, H., Gilge, S., Fricke, W., Wiegner, M., Freudenthaler, V., Gro, S., Ries, L., Meinhardt, F., Birmili, W., Münkel, C., Obleitner, F., Suppan, P., Mar. 2011. Measurement and simulation of the 16/17 April 2010 eyjafjallajökull volcanic ash layer dispersion in the northern Alpine region. Atmospheric Chemistry and Physics 11 (6), 2689–2701.

Evensen, G., May 1994. Sequential data assimilation with a nonlinear quasi-geostrophic model using Monte Carlo methods to forecast error statistics. J. Geophys. Res. 99 (C5), 10143–10162.

Evensen, G., Nov. 2003. The Ensemble Kalman Filter: theoretical formulation and practical implementation. Ocean Dynamics 53 (4), 343–367.

Evensen, G., Dec. 2004. Sampling strategies and square root analysis schemes for the EnKF. Ocean Dynamics 54 (6), 539–560.

Evensen, G., van Leeuwen, P. J., Jun. 2000. An Ensemble Kalman Smoother for Nonlinear Dynamics. Mon. Wea. Rev. 128 (6), 1852–1867.

Flemming, J., Inness, A., Sep. 2013. Volcanic sulfur dioxide plume forecasts based on UV satellite retrievals for the 2011 Grímsvötn and the 2010 Eyjafjallajökull eruption. J. Geophys. Res. Atmos. 118 (17), 10,172–10,189.

Flentje, H., Claude, H., Elste, T., Gilge, S., Köhler, U., Plass-Dülmer, C., Steinbrecht, W., Thomas, W., Werner, A., Fricke, W., Jun. 2010. The eyjafjallajökull eruption in April 2010 – detection of volcanic plume using in-situ measurements, ozone sondes and a new generation ceilometer network. Atmospheric Chemistry and Physics Discussions 10 (6), 14947–14968.

Groß, S., Gasteiger, J., Freudenthaler, V., Schnell, F., Wiegner, M., 2010. Characterization of the Eyjafjallajökull ash-plume by means of lidar measurements over the Munich EARLINET-site. Vol. 7832. SPIE, pp. 78320M–78320M–8.

Heim, M., Mullins, B. J., Umhauer, H., Kasper, G., Dec. 2008. Performance evaluation of three optical particle counters with an efficient multimodal calibration method. Journal of Aerosol Science 39 (12), 1019–1031.

Houtekamer, P. L., Mitchell, H. L., Mar. 1998. Data Assimilation Using an Ensemble Kalman Filter Technique. Mon. Wea. Rev. 126 (3), 796–811.

Jones, A., Thomson, D., Hort, M., Devenish, B., 2007. The U.K. Met Office's Next-Generation Atmospheric Dispersion Model, NAME III. In: Borrego, C., Norman, A.-L. (Eds.), Air Pollution Modeling and Its Application XVII. Springer US, pp. 580–589.

Langmann, B., 2013. Volcanic Ash versus Mineral Dust: Atmospheric Processing and Environmental and Climate Impacts. ISRN Atmospheric Sciences 2013, 1–17.

Lolli, S., Conil, S., Dabas, A., Donovan, D., Gryning, S. E., Mikkelsen, T., Ricketts, H., Sauvage, L., Vaughan, G., Walter, J., Wienhold, F., 2010. Eyjafjallajökull volcano ash plume detection in the frame of the new constituting lidar network leonet. Vol. 7832. pp. 78320K–78320K–7.

Mastin, L. G., Guffanti, M., Servranckx, R., Webley, P., Barsotti, S., Dean, K., Durant, A., Ewert, J. W., Neri, A., Rose, W. I., Schneider, D., Siebert, L., Stunder, B., Swanson, G., Tupper, A., Volentik, A., Waythomas, C. F., Sep. 2009. A multidisciplinary effort to assign realistic source parameters to models of volcanic ash-cloud transport and dispersion during eruptions. Journal of Volcanology and Geothermal Research 186 (1-2), 10–21.

Miffre, A., David, G., Thomas, B., Rairoux, P., 2010. Characterization of Iceland volcanic aerosols by UV-polarization lidar at Lyon, SW Europe. Vol. 7832. pp. 78320Q–78320Q–9.

Oberhuber, J. M., Herzog, M., Graf, H.-F., Schwanke, K., Dec. 1998. Volcanic plume simulation on large scales. Journal of Volcanology and Geothermal Research 87 (1-4), 29–53.

Pappalardo, G., Amodeo, A., Ansmann, A., Apituley, A., Alados Arboledas, L., Balis, D., Böckmann, C., Chaikovsky, A., Comeron, A., D'Amico, G., De Tomasi, F., Freudenthaler, V., Giannakaki, E., Giunta, A., Grigorov, I., Gustafsson, O., Gross, S., Haeffelin, M., Iarlori, M., Kinne, S., Linné, H., Madonna, F., Mamouri, R., Mattis, I., McAuliffe, M., Molero, F., Mona, L., Müller, D., Mitev, V., Nicolae, D., Papayannis, A., Perrone, M. R., Pietruczuk, A., Pujadas, M., Putaud, J.-P., Ravetta, F., Rizi, V., Serikov, I., Sicard, M., Simeonov, V., Spinelli, N., Stebel, K., Trickl, T., Wandinger, U., Wang, X., Wagner, F., Wiegner, M., 2010. Earlinet observations of the eyjafjallajökull ash plume over europe. Vol. 7832. pp. 78320J–78320J–9.

Schaap, M., Timmermans, R. M. A., Roemer, M., Boersen, G. A. C., Builtjes, P. J. H., Sauter, F. J., Velders, G. J. M., Beck, J. P., 2008. The LOTOS EUROS model: description, validation and latest developments. International Journal of Environment and Pollution 32 (2), 270+.

Schäfer, K., Birmili, W., Cyrys, J., Emeis, S., Forkel, R., Gilge, S., Münkel, C., Pitz, M., Ries, L., Suppan, P., 2010. Temporal and spatial structure of a volcanic ash cloud: ground-based remote sensing and numerical modeling. Vol. 7832. pp. 78320R–78320R–12.

Schumann, U., Weinzierl, B., Reitebuch, O., Schlager, H., Minikin, A., Forster, C., Baumann, R., Sailer, T., Graf, K., Mannstein, H., Voigt, C., Rahm, S., Simmet, R., Scheibe, M., Lichtenstern, M., Stock, P., Rüba, H., Schäuble, D., Tafferner, A., Rautenhaus, M., Gerz, T., Ziereis, H., Krautstrunk, M., Mallaun, C., Gayet, J. F., Lieke, K., Kandler, K., Ebert, M., Weinbruch, S., Stohl, A., Gasteiger, J., Groß, S., Freudenthaler, V., Wiegner, M., Ansmann, A., Tesche, M., Olafsson, H., Sturm, K., Mar. 2011. Airborne observations of the Eyjafjalla volcano ash cloud over Europe during air space closure in April and May 2010. Atmospheric Chemistry and Physics 11 (5), 2245–2279.

Searcy, C., Dean, K., Stringer, W., Jan. 1998. PUFF: A high-resolution volcanic ash tracking model. Journal of Volcanology and Geothermal Research 80 (1-2), 1–16.

Sparks, R. S. J., Burski, M. I., Carey, S. N., Gilbert, J. S., Glaze, L. S., Sigurdsson, H., Woods, A. W., 1997. Volcanic Plumes, 1st Edition. Wiley.

Stohl, A., Prata, A. J., Eckhardt, S., Clarisse, L., Durant, A., Henne, S., Kristiansen, N. I., Minikin, A., Schumann, U., Seibert, P., Stebel, K., Thomas, H. E., Thorsteinsson, T., Tørseth, K., Weinzierl, B., May 2011. Determination of time- and height-resolved volcanic ash emissions and their use for quantitative ash dispersion modeling: the 2010 eyjafjallajökull eruption. Atmospheric Chemistry and Physics 11 (9), 4333–4351.

Tesche, M., Ansmann, A., Hiebsch, A., Mattis, I., Schmidt, J., Seifert, P., Wandinger, U., 2010. Lidar observations of the Eyjafjallajokull volcanic ash plume at Leipzig, Germany. Vol. 7832. pp. 78320L–78320L–9.

van Velzen, N., Segers, A. J., Mar. 2010. A Problem-solving Environment for Data Assimilation in Air Quality Modelling. Environ. Model. Softw. 25 (3), 277–288.

van Velzen, N., Verlaan, M., Dec. 2007. COSTA a problem solving environment for data assimilation applied for hydrodynamical modelling. Meteorologische Zeitschrift 16 (6), 777–793.

Verlaan, M., Heemink, A. W., Oct. 1997. Tidal flow forecasting using reduced rank square root filters. Stochastic Hydrology and Hydraulics 11 (5), 349–368.

Weber, K., Eliasson, J., Vogel, A., Fischer, C., Pohl, T., van Haren, G., Meier, M., Grobéty, B., Dahmann, D., Mar. 2012. Airborne in-situ investigations of the Eyjafjallajökull volcanic ash plume on Iceland and over north-western Germany with light aircrafts and optical particle counters. Atmospheric Environment 48, 9–21.

Weber, K., Vogel, A., Fischer, C., van Haren, G., Pohl, T., 2010. Airborne measurements of the Eyjafjallajökull volcanic ash plume over northwestern Germany with a light aircraft and an optical particle counter: first results. Vol. 7832. pp. 78320P–78320P–15.

Webley, P. W., Steensen, T., Stuefer, M., Grell, G., Freitas, S., Pavolonis, M., Jul. 2012. Analyzing the Eyjafjallajökull 2010 eruption using satellite remote sensing, lidar and WRF-Chem dispersion and tracking model. Journal of Geophysical Research 117.

Webley, P. W., Stunder, B. J. B., Dean, K. G., 2009b. Significant eruption source parameter(s) for operational ash cloud transport and dispersion models 186(1-2), 108–119.

Witham, C. S., Hort, M. C., Potts, R., Servranckx, R., Husson, P., Bonnardot, F., Mar. 2007. Comparison of VAAC atmospheric dispersion models using the 1 November 2004 Grimsvötn eruption. Met. Apps 14 (1), 27–38.

Zehner, C. (Ed.), May 2010. Monitoring Volcanic Ash From Space. ESA communication Production Office.

Zhang, L., 2001. A size-segregated particle dry deposition scheme for an atmospheric aerosol module. Atmospheric Environment 35 (3), 549–560.

Research Highlights:

- Aircraft-based measurements are assimilated into a volcanic ash transport model.
- Assimilation can significantly improve the state of ash clouds and ash forecast.
- Measurements should be preferably taken from the same level with aeroplane flying.
- Uncertainty knowledge of ESPs and measurements is important for aviation advice.

ACCEPTED MANUSCRIPT